Acta Biomaterialia 73 (2018) 365–376

Contents lists available at ScienceDirect

Acta Biomaterialia

journal homepage: www.elsevier.com/locate/actabiomat

Full length article

Electrospun silk fibroin fibers for storage and controlled release of human platelet lysate

Cataldo Pignatelli [a,b,*,1], Giovanni Perotto [a,*,1], Marta Nardini [c,d], Ranieri Cancedda [c,d], Maddalena Mastrogiacomo [c,d], Athanassia Athanassiou [a,*]

[a] Smart Materials, Istituto Italiano di Tecnologia, via Morego 30, 16163 Genoa, Italy
[b] DIBRIS, University of Genoa, via Opera Pia 13, 16145 Genoa, Italy
[c] Department of Experimental Medicine (DIMES), University of Genova, Largo Rosanna Benzi 10, 16132 Genova, Italy
[d] IRCCS AOU San Martino–IST Istituto Nazionale per la Ricerca sul Cancro, Largo Rosanna Benzi 10, 16132 Genova, Italy

ARTICLE INFO

Article history:
Received 12 October 2017
Received in revised form 31 March 2018
Accepted 12 April 2018
Available online 17 April 2018

Keywords:
Silk fibroin
Human platelet lysate
Electrospinning
Controlled release
Shelf-life
Regenerative medicine

ABSTRACT

Human platelet lysate (hPL) is a pool of growth factors and cytokines able to induce regeneration of different tissues. Despite its good potentiality as therapeutic tool for regenerative medicine applications, hPL has been only moderately exploited in this field. A more widespread adoption has been limited because of its rapid degradation at room temperature that decreases its functionality. Another limiting factor for its extensive use is the difficulty of handling the hPL gels. In this work, silk fibroin-based patches were developed to address several points: improving the handling of hPL, enabling their delivery in a controlled manner and facilitating their storage by creating a device ready to use with expanded shelf life. Patches of fibroin loaded with hPL were synthesized by electrospinning to take advantage of the fibrous morphology. The release kinetics of the material was characterized and tuned through the control of fibroin crystallinity. Cell viability assays, performed with primary human dermal fibroblasts, demonstrated that fibroin is able to preserve the hPL biological activity and prolong its shelf-life. The strategy of storing and preserving small active molecules within a naturally-derived, protein-based fibrous scaffold was successfully implemented, leading to the design of a biocompatible device, which can potentially simplify the storage and the application of the hPL on a human patient, undergoing medical procedures such as surgery and wound care.

Statement of Significance

Human platelets lysate (hPL) is a mixture of growth factors and cytokines able to induce the regeneration of damaged tissues. This study aims at enclosing hPL in a silk fibroin electrospun matrix to expand its utilization. Silk fibroin showed the ability to preserve the hPL activity at temperature up to 60 °C and the manipulation of fibroin's crystallinity provided a tool to modulate the hPL release kinetic. This entails the possibility to fabricate the hPL silk fibroin patches in advance and store them, resulting in an easy and fast accessibility and an expanded use of hPL for wound healing.

1. Introduction

Silk fibroin, a structural protein of the cocoons of the *Bombyx mori*, is widely studied for biomedical applications, such as tissue regeneration and drug delivery, because it is biocompatible, resorbable and can be fabricated in multiple formats [1–3]. The extraction of fibroin from the cocoons, a process known as regeneration, results in an aqueous solution that can be used to fabricate films, hydrogels, sponges, nanoparticles and fibers [1–8]. Silk fibroin self-assembles from the water solution into an amorphous state (called silk I) presenting α-helices, and a crystalline state (called silk II) with high β-sheets content [2,9,10]. The β-sheets characterizing silk II affect several of its physical and chemical properties, such as mechanical strength and refractive index [11,12]. Particularly interesting is the water stability provided by

* Corresponding authors at: Smart Materials, Istituto Italiano di Tecnologia, via Morego 30, 16163 Genoa, Italy (Giovanni Perotto).
E-mail addresses: cataldo.pignatelli@iit.it (C. Pignatelli), giovanni.perotto@iit.it (G. Perotto), athanassia.athanassiou@iit.it (A. Athanassiou).
[1] These authors equally contributed to the work.

https://doi.org/10.1016/j.actbio.2018.04.025
1742-7061/

the β-sheet secondary structure: while silk I is soluble in water, highly crystalline silk II does not dissolve in pure water [13]. The transition from the amorphous state silk I to the crystalline silk II can be favored by using alcohols or via water vapor annealing [13–15]. The crystallization assisted by water vapor is slower, more controlled and it allows to obtain different crystallinity degrees by varying the treatment duration. Being a milder process, water vapor annealing can be applied even when sensitive molecules or cellular organelles are embedded in fibroin matrices [13,16–28]. Crystallinity manipulation of fibroin was used as a processing strategy to tune its biodegradability and to control the release of drugs. *In vitro* enzymatic degradation assays, performed on fibroin fibrous scaffolds, have shown a slower degradation rate when the scaffold presented high crystallinity [8,29,30]. *In vivo* studies confirmed the longer permanence of highly crystalline silk fibroin implants [31]. The control on the degradation is especially interesting in drug delivery applications, since controlling the rate of degradation enables the prolonged and sustained delivery of active factors during the entire course of the therapy. Investigations *in vitro* with highly crystalline silk fibroin matrices (>40% crystallinity) showed a slower release compared to the amorphous silk [20,32–35]. The ability of the silk fibroin in controlling the release was found also *in vivo* using chemotherapeutic agents. They were released in a sustained way and this kept their concentration under toxic threshold [19,36]. On the top, such controlled delivery can keep the overall drug concentration low within the patient's body, reducing the frequency of the treatment administration as well [37]. Within the context of regenerative medicine, the sustained release of growth factors from biodegradable polymeric matrices showed an accelerated and improved wound healing and a great potential for more complete cells differentiation in tissue engineering [38–40]. Also for chronic wounds, keeping low the concentration of growth factors and for longer time, can help their healing [41,42].

Human platelets lysate (hPL) is a potential therapeutic tool highly enriched with platelets-derived growth factors and cytokines. Although there are no publications reporting the exact and total content of single components of the hPL, many articles have described some of the growth factors included: platelet-derived growth factor B (PDGF-BB), fibroblasts growth factors (FGF), vascular endothelial growth factor (VEGF), epidermal growth factors (EGF) and transforming growth factor-B 1 (TGF-β1) [43–45]. Such growth factors are physiologically involved in regenerative and healing processes. *In vitro* experiments have shown the hPL ability to support every stage of the wound healing: favoring cells growth, angiogenesis and stimulating the recruitment of white blood cells [46–48]. *In vivo* experiments showed its ability to support bone regeneration and the recovery of non-healing wounds [49,50]. hPL is commonly applied in the form of a gel, which can release the platelets-derived factors [51]. Despite these promising results, on-the-spot preparation, difficult handling, need of storage at low temperature to preserve the activity of the factors are some of the technical and practical limitations that still hinder the hPL usage as therapeutic tool [52,53]. Therefore, there is a need of designing a device that could conjugate the sustained release of the allogenic hPL with an easier handling on a wound, while keeping the hPL factors well-preserved. This would allow a more effective use of the hPL molecules in the wound care management.

The aim of this work is the creation of a device that is able to take advantage of several properties of silk fibroin such to facilitate and expand the use of hPL. In particular, silk fibroin provides a matrix that can be processed in conditions that are compatible with hPL (in water, at room temperature and at neutral pH) [3] and that can be fabricated in micro and nanofibers using electrospinning [54,55]. In addition, the possibility to control the silk fibroin crystallinity could be used as a mechanism to tune the release kinetic [32,33,56]. Silk fibroin has shown the ability to stabilize sensitive molecules and cell organelles [16–18,21–27,57], and, building on this, the present work investigates how to exploit this property to facilitate the use of hPL. Herein, the hPL was encapsulated in silk fibroin electrospun fibers. The electrospun format was chosen because the porosity, granted by the micro and nanofibers, facilitates both the absorption of exudate and an efficient gas exchange, while supporting cell proliferation and migration. All the above mentioned features successfully mimic the natural extracellular matrix, thus improving and sustaining the healing process of the wounds [58–61].

Silk fibroin fibers with a high content of hPL were fabricated, and their degradation and release kinetics were controlled via manipulation of the fibroin crystallinity. The release kinetics of the silk fibroin fibrous mats with different crystallinity degrees were characterized tracking the release of albumin [62,63] using an *in vitro* test that was developed to simulate *in vivo* degradation conditions. Enzyme-linked immunosorbent assay (ELISA) was performed to prove that the crystallinity of silk fibroin could control the release kinetics of two of the hPL growth factors: PDGF and TGF-β1. Furthermore, hPL released from silk fibroin fibers retained its ability to induce and sustain the viability of primary adult human dermal fibroblasts (HDFa) *in vitro*. Finally, the possibility to use silk fibroin for the preservation of hPL biological activity was proved even after thermal stress at 60 °C [25,28], demonstrating the improvement of the shelf-life of hPL, granted by the fibroin matrix. Such system can be proposed as a valid, easy-to-fabricate and durable alternative to the platelet-rich plasma (PRP) gel in the wound care management.

2. Materials and methods

2.1. Materials

Sodium carbonate, sodium chloride, lithium bromide, poly (ethylene oxide) (PEO, M_w = 1,000,000 g/mol), albumin conjugated with fluorescein isothiocyanate (FITC-albumin), phosphate buffer saline (PBS), Protease XIV (≥4 units/mg), paraformaldehyde (PFA) and bovine serum albumin (BSA), Triton X-100 were purchased from Sigma Aldrich (MO, USA). ELISA kit for the detection of Human PDGF-BB was purchased from RayBiotech Inc (GA, USA); ELISA kit for the detection of Human TGF-β1 was purchased from Invitrogen (CA, USA). Human dermal fibroblast from adult (HDFa), medium 106, low serum growth supplement kit, trypsin, trypsin neutralizer, Alexa Fluor™ 488 Phalloidin and ProLong™ Diamond Antifade Mountant with DAPI were purchased from ThermoFisher Scientific (MA, USA). Cell proliferation reagent WST-1 (2-(4-iodo phenyl)-3-(4-nitophenyl)-5-(2,4-disulfophenyl)-2H-tetrazolium monosodium salt) was purchased from Roche (Switzerland). Finally, hPL was gently granted by Biorigen s.r.l. (Italy).

2.2. Fibroin regeneration and hPL preparation

Fibroin was extracted from *Bombyx mori* cocoons according to the protocol previously described by Rockwood *et al.* [3]. Firstly, the cocoons were cut and boiled for 30 min in a water solution of 0.023 M of Na_2CO_3; subsequently, the fibers were washed with MilliQ (18.3 MΩ) water and dried. Degummed fibroin was solubilized in an aqueous solution of 9.3 M of lithium bromide at 60 °C for 4 h and dialyzed in a tube with a MWCO of 3,500 kDa for 3 days against MilliQ water. Finally, regenerated fibroin was centrifuged twice at 9000 rpm, for 20 min at 4 °C. To quantify the fibroin concentration, 1 mL of regenerated fibroin solution was left to dry under an aspirating hood. Then, the dried film was weighted,

obtaining the concentration of silk fibroin in the solution. The concentration was found to be in a range between 60 and 80 mg/mL.

hPL used in this work, provided by Biorigen s.r.l., was prepared according to the method described by Zaky *et al.* [43]. Briefly, the PRP obtained from buffy coat samples from the whole blood of healthy donors, has undergone freeze–thaw cycles in order to break the platelet membranes and to release their growth factors content. The supernatant hPL recovered was freeze-dried. It contained platelet growth factors with different size. To reduce or avoid the variability from batch to batch, each single batch was derived from 400 donors. hPL was standardized among batches, by making sure that PDGF-BB and VEGF concentrations were constant [44,45].

2.3. Fibers fabrication and water vapor treatment

To produce the fibers, fibroin 60 mg/mL solution was used. To facilitate the electrospinning process and fabricate the fibers, PEO powder 25% (w/w_{silk}) was added to a 60 mg/ml aqueous solution of fibroin and stirred overnight. Generally, to electrospin silk fibroin, PEO is added because it adjusts the viscosity of the regenerate silk fibroin, as reported in previous works [54,64–66]. Once a homogeneous solution was obtained, FITC-albumin powder was added such to obtain a concentration of 2% (w/w_{silk}). To add hPL, a solution of it 7% (w/w_{silk}) was added to not diluted silk fibroin solution. Therefore, hPL solution needs to have an enough volume to dilute the silk fibroin solution at 60 mg/mL. The final concentration of the hPL in the electrospun fibers was 5% (w/w). The fibers were electrospun at 20 °C in a controlled humidity environment (30%–40% relative humidity) with a syringe pump (NE-1000, New Era Pump Systems, Inc., NY, USA) equipped with a blunt 19G needle, at a flow rate of 1 mLh^{-1} (Fig. S1A). An aluminum, grounded collector was placed at 20 cm from the needle, while a voltage of 18 kV was applied (EH40R2.5, Glassman High Voltage, Inc., US-NJ, USA). In the case of the hPL loaded fibers, the following parameters were considered: a flow rate of 1.2 mLh^{-1}, a needle–collector distance of 30 cm, and a voltage of 23 kV. These parameters were optimized for the different compositions in order to have a continuous electrospinning process and to produce beads-free fibers.

The crystallinity degree of the silk fibroin fibrous mats was increased via water vapor annealing. The treatment was performed in a vacuum oven (VO500EA, MLS, Italy) at 40 °C and 85–90% of relative humidity. Different treatment times were used for the different crystallization reported (Fig. S1B), ranging from 10 min to 6 h.

2.4. Fiber characterization

2.4.1. Morphology

Fiber morphology was characterized by scanning electron microscopy (SEM) using a JEOL JSM-6490LA microscope (JEOL Ltd., Japan), in high vacuum with an acceleration voltage of 15 kV. The samples were previously coated with a 10-nm-thick gold layer with a Cressington 208HR high resolution sputter coater (Cressington Scientific Instrument Ltd, U.K.). Size analysis was performed with ImageJ software.

2.4.2. Drug encapsulation

The encapsulation of the hPL in the fibers was investigated through the detection of the FITC-albumin, PDGF and TGF-β1. FITC-albumin was observed by using a laser scanning confocal microscope (A1R, Nikon, Japan). The lasers had wavelengths of 401–488 nm (Nikon, Japan). To evaluate the encapsulation of the PDGF and TGF-β1, low crystalline fibrous mats were dissolved in PBS 0.04 M pH 7.4 at 37 °C for 24 h, to ensure a complete release of hPL. Then, the releasing media were evaluated through the ELISA kits to quantify the PDGF and TGF-β1, according to the manufacturer's instructions.

2.4.3. Fibroin crystallinity characterization

Characterization of the fiber crystallinity was performed by Fourier transform infrared spectroscopy (FTIR). Samples were measured in Attenuated Total Reflectance (ATR) mode using MIRacle ATR accessory (PIKE Technologies, WI, USA) coupled to a Fourier Transform Infrared (FTIR) spectrometer (Equinox 70 FT-IR, Bruker, MA, USA). All the spectra were acquired in a spectral range from 4000 to 600 cm^{-1}, with a scanning resolution of 4 cm^{-1}, accumulating 64 scans.

The deconvolution of the fibroin amide I peak was performed as reported previously by Guzman-Puyol *et al.* and Hu *et al.* [67,68]. The software was PeakFit 4.11 [67] and the wavenumber positions of the different components were deduced by calculation of the second-order derivative [68]. The fitting of the different contributions was performed using Gaussian-shaped peaks, using an equal fixed width for all the considered peaks. The crystallinity content was obtained from the ratio between the areas of the β-sheets peaks and the total area of the amide I peak.

2.4.4. Drug release assessment

Electrospun silk fibroin unloaded (SF), loaded with FITC-albumin (SF-alb), loaded with hPL (SF-hPL), and loaded both with FITC-albumin and hPL (SF-alb-hPL) fibers, were weighted and placed in a 24 well-plate with 1 mL of PBS 0.04 M at pH 7.4 and with 6.25 mU of Protease XIV in 0.04 M PBS pH 7.4 at 37 °C and gently stirred on a tilting plate for 5 months. At given time points, the total volume was taken out and substituted with fresh medium. The amount of FITC-albumin was determined by correlating the absorbance at 495 nm with a calibration curve measured by using the same media, after subtraction of blank spectra obtained by measuring the SF and SF-hPL samples. The measurements were carried out using a UV–visible spectrophotometer (Cary 6000i-Varian, CA, USA) from 450 nm to 550 nm.

To characterize the effect of the enzymatic degradation on the samples, three SF-alb-hPL mats having different crystallinity (22%, 35% and 45%) were incubated at 37 °C for 1 month, either with PBS or in the presence of PBS containing the enzyme (6.25 mU/mg_{fibers}). The medium was completely replaced every day. At the end of the experiment, the mats were washed with MilliQ water for 10 min five times, in order to remove traces of salt and enzyme. After the final timepoint, the samples were rinsed, dried and imaged by SEM.

The release kinetics of PDGF and TGF-β1 from SF-hPL mats with different crystallinity (20%, 35% and 44%) were characterized by quantifying the growth factors in the releasing medium. SF mats were used as control. The experiment was carried out in a protease-free buffer, in order to avoid the possible interference between the protease and the antibodies used for the ELISA procedure. Since the albumin results have shown that the sustained release (after 24 h) is mainly caused by the proteolytic degradation of the fibroin matrices, the release kinetic of the growth factors was limited to the first 120 h. The fibers were incubated for 5 days in PBS 0.04 M pH 7.4 at 37 °C on a tilting plate. At given time point, the total volume of the releasing medium was removed and substituted with fresh medium. The media, corresponding to each time points, were stored at -20 °C until they were analyzed by the ELISA. The ELISAs were performed according to the manufacturer's instructions.

2.5. Biological activity of the released hPL

Primary human dermal fibroblasts from an adult donor (HDFa) were seeded in medium 106, containing 2% (v/v) of fetal bovine

serum (FBS), 1 μg/mL of hydrocortisone, 10 ng/mL human epidermal growth factor, 3 ng/mL of basic fibroblast growth factor, and 10 μg/mL of heparin. The cells were split every 7 days and seeded at a density of 4500 cells/cm^2. Medium was changed every day.

To assess the retained activity of the released hPL, 20 mg of SF and SF-hPL fibers, at 24% of crystallinity, were incubated, after sterilization with UV treatment for 20 min for each side, in 4 mL of serum-free culture medium for 24 h at 37 °C. The low crystallinity of the mats permitted the dissolution of the matrix and the complete release of all the factors in 24 h. The size of silk fibroin mats dissolved in the serum-free culture medium, was cut in order to release 250 μg/mL of hPL in the media. This concentration was chosen because, as observed in a dose–response experiment (Fig. S8), it was found to be the minimum concentration able to increase the viability of the HDFa. Twenty-four hours before the treatment, cells were seeded with a density of 4500 cells/cm^2 in complete culture medium. The day after, some cells were used to assess the viability before the treatment with the samples. This reading was labeled time point zero. The rest were washed with PBS and incubated according to the following conditions: SF extracts, SF-hPL extracts, culture media containing the same hPL amount released from the SF-hPL, and serum-free culture media and complete culture media as controls. Cells viability was evaluated through the analysis of the cell metabolism, thanks to a colorimetric assay. WST-1 was directly added in culture medium with a 1:11 (v/v) ratio. After the addition of the WST-1, the cells were incubated for 3 h, at 37 °C with and 5% of CO_2. The assay was performed after 1, 3, and 5 days of treatment, acquiring the absorbance at 450 nm, through a multiwell plate reader (Multiskan™ GO Microplate Spectrophotometer, ThermoFisher scientific, MA, USA) and normalizing all the outcome signals with respect to the absorbance value at the zero-time point.

2.6. Improvement of hPL shelf-life

With the aim of mimicking an aging process, an oven treatment at 60 °C was performed on SF and SF-hPL samples, lyophilized hPL and on aliquots of plain and hPL-containing serum-free culture media. Lyophilized hPL represents the common way for storage; hPL dissolved in serum-free culture media mimics the common "device" use of hPL: the platelet gel; SF-hPL is the ready-to-use silk fibroin-based device. 60 °C were used because it is a temperature at which labile molecules, like hPL proteins, are known to degrade and because it is a temperature used in previous works to test the improvement of stability granted by silk fibroin [25,28]. The electrospun mats were cut to be 20 mg in mass, containing 1 mg of hPL each and were dissolved, after the oven treatment and 20 min of UV sterilization cycle for each side, in 4 mL of serum-free culture media for 24 h at 37 °C, to release the encapsulated hPL and prepare the extract for the following cell experiments. All the electrospun samples were 24% crystalline, so they fully dissolved during the 24 h incubation. For the control samples, lyophilized hPL was dissolved in the serum-free medium in order to have the same concentration of the electrospun samples (250 μg/ml). Three treatment time points were investigated: 24 h, 48 h and 72 h. HDFa cells were seeded onto 96-well plates at a density of 4500 cells/cm^2 and let attached overnight. The next morning, cells were treated with the prepared extracts from the thermally treated samples above listed. WST-1 viability assay was performed after 5 days, acquiring the absorbance at 450 nm and normalizing all the outcome signals with respect to the absorbance value of the negative control (medium without serum and hPL). The residual activity of the hPL was calculated from the ratio of the cell viability observed in the case of the thermally treated mats and the cell viability in the case of the untreated samples.

2.7. Cells morphology

To evaluate the morphology of the cells directly seeded onto the fibrous mats, electrospun silk fibroin fibers were collected on 14 mm coverslips and treated with water vapor for 10 min, as previously explained. After UV sterilization for 20 min, HDFa were seeded on SF and SF-hPL matrices and observed under the confocal microscope after 1, 3 and 5 days of growth. Cells were washed twice with PBS, fixed with PFA 4% for 10 min, and treated with Triton X-100 0.1% in PBS for additional 10 min. Afterwards, the samples were incubated with a blocking solution of 1% BSA in PBS for 20 min and then stained with Alexa Fluor™ 488 Phalloidin (diluted 1:40 in 1% BSA) for 20 min. All the steps were performed at room temperature. Finally, the cells were mounted on glass slide with ProLong™ Diamond Antifade Mountant containing DAPI for nuclear staining and stored at 4 °C.

2.8. Statistical methods

The fibers size analysis was performed on three samples for each fibrous formulation (SF, SF-alb, SF-hPL and SF-alb-hPL) before and after the water vapor annealing. The average of size measurements (n = 400) was obtained along the respective standard error.

Three samples of each fibrous sample and each condition (not treated, treated for 10 min and treated for 6 h with water vapor) were used for FITR analysis, acquiring 5 spectra from each of them, which were averaged to obtain the final spectrum for the deconvolution. The same samples (three for each crystallinity degree and three for each fibers type) were used to investigate the release. The average of the release from the triplicates was obtained with the respective standard error. The quantification of the PDGF and TGF-β1 released from the fibrous mats was performed by using the respective ELISA kits. For the encapsulation analysis, 3 low crystalline mats were used, while, for characterizing the release kinetics, 3 different samples for each crystallinity were used. The averages with the respective standards errors were obtained for both the experiments. The cell viability assays were repeated 3 times for each fibrous sample. The average with the respective standard error was obtained. For viability assays, the statistics were performed through the analysis of variance (ANOVA), followed by *post-hoc* Bonferroni correction. A value of $p \leq 0.05$ was considered statistically significant.

3. Results

3.1. Fibers fabrication and characterization

In Fig. 1 and Fig. S2 electrospun mats SF, SF-alb, SF-hPL, SF-alb-hPL are presented. The fibers were defect-free, showing a smooth morphology. Their average diameter was measured to be 370 ± 3 nm, 330 ± 2 nm, 360 ± 3 nm, and 480 ± 2 nm, respectively. After the water vapor treatment was performed, no statistically significant change in the average diameter was observed, with dimensions of 400 ± 4 nm, 370 ± 3 nm, 480 ± 4 nm, and 530 ± 8 nm, respectively.

Although different electrospinning parameters were used, the size and the morphology of the fibers did not significantly change with the addition of the FITC-albumin or hPL. Up to 5% (w/w) of hPL was loaded in the fibers, while above this amount, the process became less continuous and reproducible.

After the water vapor treatment, the surface of the single fibers resulted smooth, indicated that such treatment did not induce modifications on their surface. On the other hand, it induced the

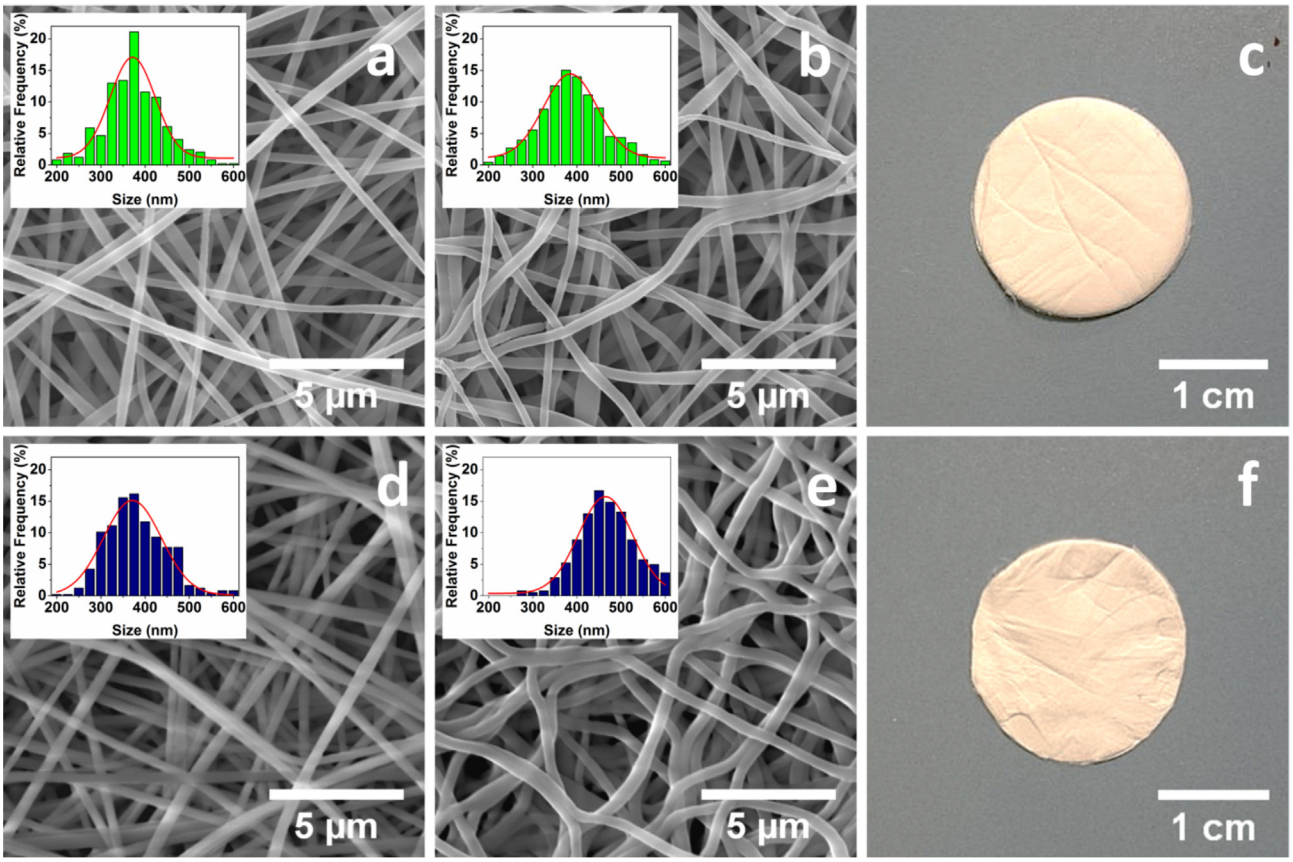

Fig. 1. SEM images of SF (a and b) and SF-hPL (d and e) fibers mats obtained by electrospinning. The fiber morphology is characterized before (a and d) and after (b and e) the water vapor treatment. The insets show the corresponding size distributions. Photos of the obtained electrospun SF (c) and SF-hPL (d) fibrous mats.

flattening of the fibers in all the formulations, an effect often associated with post treatment of fibroin fibers (Fig. 1) [69,70].

FITC-albumin was used as a tracer to characterize the release kinetic from the electrospun fibers, since albumin is one of the elements of hPL (Fig. S3) [62,63]. The successful encapsulation was verified with a confocal microscope, through the FITC fluorescence (Fig. 2). The distribution of the fluorescence signal appeared homogenous along the fibers and no differences were observed when the hPL was added to the system (Fig. 2).

The encapsulation of PDGF and TGF-β1 in the electrospun fibers was confirmed by ELISA: samples contained 128 ± 25 pg of PDGF and 769 ± 85 pg of TGF-β1 per mg of fibrous mat.

Silk fibroin's secondary structure (i.e. the formation of β–sheets domains) is important to tailor the release kinetics from the electrospun samples. To characterize it together with the modifications induced by water vapor annealing, the amide I peak was analyzed by FT-IR and reported in Fig. 3 [13]. The peak of the non-treated fibrous mats was centered at 1651 cm^{-1}. After 10 min of water vapor treatment, the spectra showed a change in the peak shape, with a shoulder at 1628 cm^{-1}, while a further shift to 1624 cm^{-1} was noticed after 6 h treatment. These changes can be associated to an increase in the β-sheets formation, as reported previously by Hu *et al.* [68].

The crystallinity degree was calculated for each sample through the deconvolution of the amide I peak. As expected, non-treated electrospun fibers showed a β-sheets content ranging from 21% to 24%. On the other hand, fibers treated for 10 min presented a crystallinity degree of 34–36%, while those undergoing water vapor annealing for 6 h reached up to 44–46% of crystalline phase.

3.2. Drug release assessment

3.2.1. Characterization of the drug release

To precisely assess the release kinetics for all the crystallinities explored, a release medium with proteolytic enzymes was developed in order to simulate the *in vivo* enzymatic degradation. Protease XIV was used as proteolytic enzyme. Such Protease is commonly used as enzyme for comparing the degradation properties of the silk fibroin [71,72]. The quantity of the protease was selected, after testing several concentrations, to ensure that the time of degradation of the fibroin in the release medium would have the same kinetics reported in literature for the biodegradation *in vivo*. To select the protease concentration, 6.25 mU/mg_{fibers} and 250 mU/mg_{fibers} were tested (Fig. S6). The 6.25 mU/mg_{fibers} was chosen because it resulted in a degradation time of 10 months, comparable to previous data reported in literature on the silk fibroin biodegradation *in vivo* [31,73].

Fig. 4 shows the release profiles of FITC-albumin from the fibrous mats, with different crystallinity, over a period of 5 months. The results are summarized in Table 1. The study was performed on both SF-alb and SF-alb-hPL mats. In both cases, the fibers presenting the lowest crystallinity were totally dissolved within 1 h and all the encapsulated FITC-albumin was completely released. During the initial burst, the samples with about 30% crystallinity released 41 ± 2%–48 ± 2% of the loaded FITC-albumin. A strikingly different behavior in this initial phase was observed for the samples with 45% of crystallinity, which released only 6 ± 0.2%–10 ± 0.7% of the total loaded FITC-albumin. After the initial burst, the release continued with a slower rate for all the samples. For

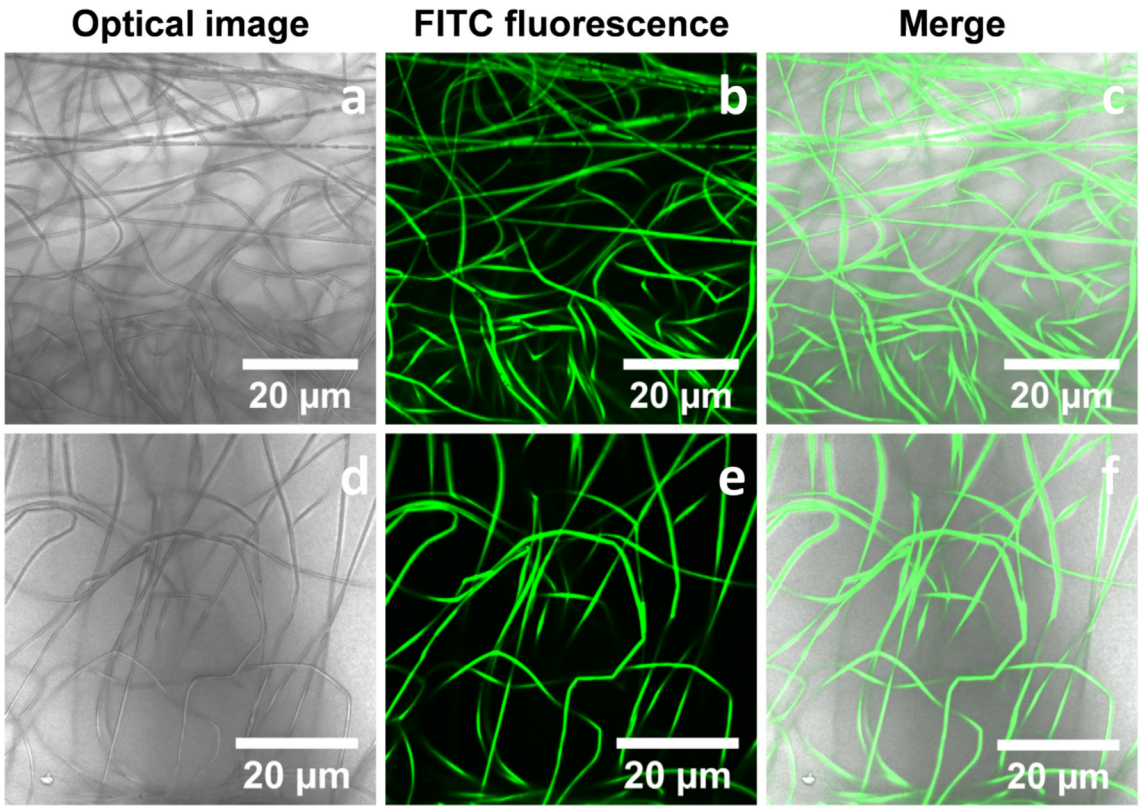

Fig. 2. Confocal microscope images of SF-alb (a, b and c), and SF-alb-hPL (d, e and f).

example, after 25 days SF-alb samples with 33% of crystallinity showed a release of 90 ± 0.3%, while samples with crystallinity of 46% released 38 ± 1% of the total FITC-albumin (Fig. 4a). Similarly (Fig. 4b), for the SF-alb-hPL samples, a release of 80 ± 2% was observed from the mats with 35% of crystallinity, while a release of 46 ± 1% was observed from the 44% crystalline mats. As shown in Fig. S7, this sustained phase of the release was absent in all the samples when the Protease XIV was not used during the experiment, and a plateau at the end of the 24 h burst was observed.

In Fig. 5, SEM images show the fibers morphology of mats with different crystallinity incubated with and without the enzyme for 1 month. The morphology of the fibers without the enzyme was preserved, unlike those incubated with the enzyme, confirming the destructive activity of the Protease XIV towards the fibroin. The loss of the fibers' morphology was higher when the crystallinity was low. The effect of slower degradation of silk fibroin by Protease XIV caused by the increased crystallinity was observed also by Gil *et al.*[72]. They attributed this effect to the slower diffusion of the enzyme in the amorphous fibroin phase. In fact, after its crystallization, supramolecular interactions in the amorphous silk fibroin increases, such to create a more organized structure, which retards the passage of the enzyme through the crystalline domains. The results in Fig. 5 are in agreement with the model they proposed, confirming also that this crystalline dependent degradation drove the second phase of the release.

3.2.2. Characterization of the PDGF and TGF-β1 release

Since the hPL activity is principally due the growth factors, the release kinetics of two of the main growth factors of the hPL, PDGF and TGF-β1, were evaluated. The experiments were performed on three mats with different crystallinity, to investigate how the different crystallinities influence the release of these growth factors. Fig. 7a and b show the burst release of the PDGF and TGF-β1 respectively. The results are summarized in Table 2. When the fibrous mats had the lowest crystallinity, 20%, the PDGF and TGF-β1 were completely released due to the total dissolution of the fibers. When the crystallinity of the fibrous mats was 35%, the PDGF released was 78 ± 9% after 24 h, while when the crystallinity was 44%, the PDGF released was 62 ± 3%, after 24 h. The TGF-β1 released was 40 ± 12% after 24 h, when the mat was 35% crystalline, while, when the mat was 44% crystalline, it was 12 ± 2% after 24 h. These results suggested that in the initial burst (24 h), as for the albumin (Fig. 7c), the release kinetics of the PDGF and TGF-β1 can be tuned by controlling the crystallinity of fibroin. In addition, the release kinetic of the PDGF resulted faster than the TGF-β1 and the albumin ones.

3.3. Biological activity of released hPL

To verify the activity of the hPL encapsulated in the fibers, low crystalline SF and SF-hPL samples were incubated in serum-free culture media, for 24 h. The Protease XIV was not used, since the sample completely dissolved in the media thanks to their low crystallinity. Fig. 8a shows the viability of HDFa cells treated with media containing the dissolved fibers. As control samples, cells were seeded in serum-free medium (labeled as negative control), or in serum-free medium in which lyophilized hPL was dissolved (labeled hPL), or in media with serum (labeled FBS). The amount of lyophilized hPL in the control was the same as the one released from SF-hPL fibers (250 μg/mL). This concentration, from the results showed in Fig. S8, resulted sufficient to observe an increase in HDFa viability. The absorbance values of all the days were normalized on the absorbance values relative to the zero-time point. After the first day of treatment, cells cultivated in media with

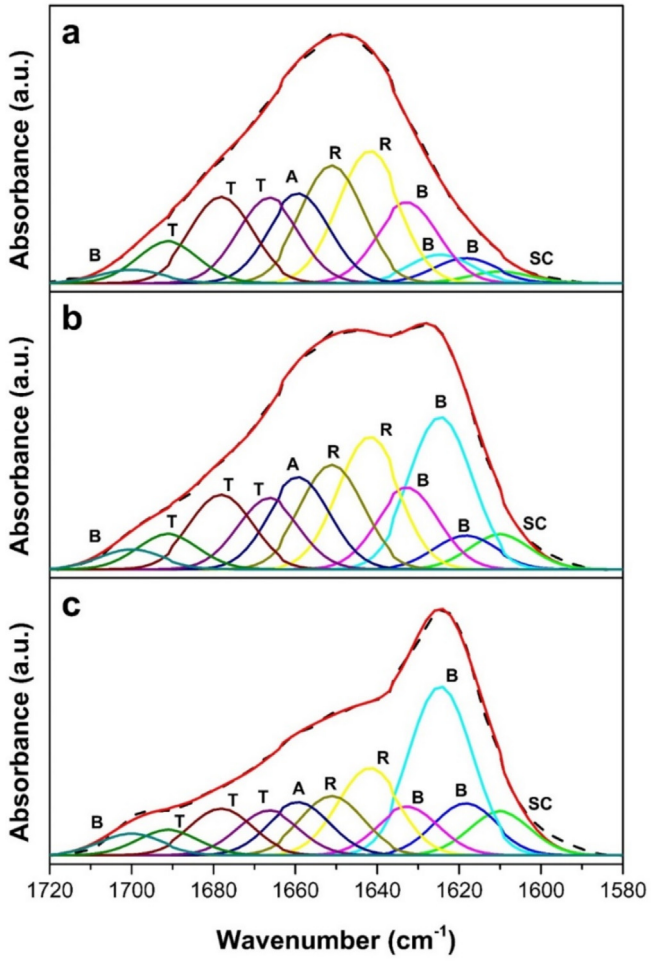

Fig. 3. Deconvoluted FT-IR spectra of the amide I band of non-treated fibers (a), fibers treated for 10 min (b), and fibers treated for 6 h (c). The crystallinity content for these samples are 21%, 34%, and 45%, respectively. SC = side chains; B = β-sheets; R = random coils; A = α-helices; T = turns.

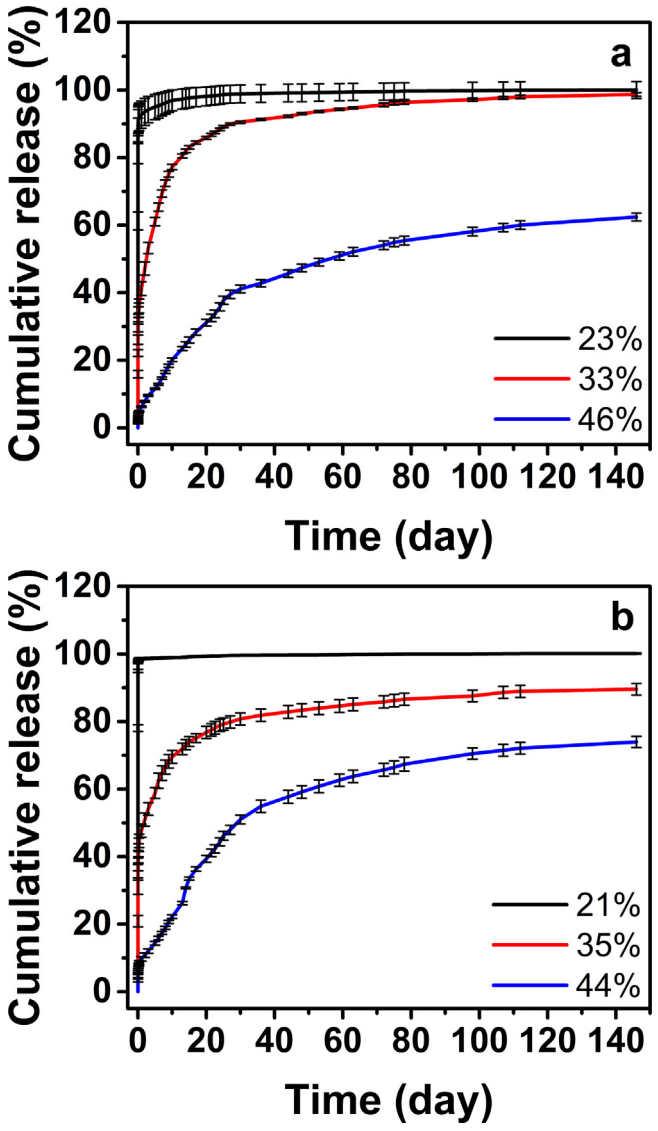

Fig. 4. FITC-albumin release kinetics: (a) SF-alb and (b) SF-alb-hPL electrospun fibers. The percentages indicate the crystallinity of the fibrous mats. The release medium contained Protease XIV, to simulate the in-vivo degradation.

hPL –hPL and SF-hPL samples–had the same increase in the viability ($p > 0.05$). They resulted two-fold higher than the negative control ($p < 0.0001$). This higher viability can be associated to the cell proliferation induced by the hPL, as reported in previous work [74]. These trends were confirmed after three and five days. Silk fibroin produced no effects on the cells viability, confirming that the increase of the cell viability is due the hPL released from the fibroin fibers. Therefore, these results proved that the growth factors released from the SF-hPL were still active and that they could increase and sustain the cells viability of the HDFa cells for up to 5 days.

3.4. Cells morphology

To evaluate the role of the hPL in cell adhesion and morphology, HDFa were seeded on the SF and SF-hPL mats for 1, 3 and 5 days (Fig. 8b, c and S10). Intermediate crystalline fibrous mats (about 30% crystallinity) were used, in order to avoid their dissolution and allow the cells to attach. As visible from Fig. 8b and c, the cells attached onto SF mats after 5 days, mostly showed a rounded morphology, while, when seeded onto SF-hPL fibers, the cells appeared more elongated. Moreover, the presence of the hPL in the fibers seemed to accelerate cellular adhesion processes. Control samples on flat films with the same composition of the SF-hPL fibers, shown in Fig. S11, confirmed that the elongated morphology was caused by the hPL encapsulated in the fibers.

3.5. hPL shelf-life

To test if the activity of hPL growth factors can be preserved via encapsulation in silk fibroin fibers, an accelerated stability test was performed, inducing a thermal stress at 60 °C [25,28]. Three conditions were tested: lyophilized hPL, hPL dissolved in serum-free medium and SF-hPL. As shown in Fig. 9, the activity of the free hPL in solution was reduced at 66 ± 3% after 1 day of thermal treatment and it decreased to 41 ± 2% after 3 days. The lyophilized hPL, showed an activity of 76 ± 2% after three days of treatment. On the other hand, the activity of the hPL released from the SF-hPL mats, thermally treated for three days, was 88 ± 6%. It resulted statistically more active than the lyophilized hPL ($p < 0.05$) and the dissolved hPL ($p < 0.0001$), demonstrating the ability of silk fibroin to preserve the functionality of the encapsulated molecules even at temperatures that are expected to denature the labile hPL components.

Table 1
Summary of the release kinetics of FITC-albumin from SF-alb and SF-alb-hPL samples reported in Fig. 4.

Samples	Crystallinity	Burst release 0–24 h	Sustained release 1–25 d	Sustained release 26–146 d
SF-alb	23%	98 ± 2%	–	–
	33%	41 ± 2%	90 ± 0.3%	99 ± 0.5%
	46%	6 ± 0.2%	38 ± 1%	62 ± 1%
SF-alb-hPL	21%	99 ± 0.4%	–	–
	35%	48 ± 2%	80 ± 2%	90 ± 2%
	44%	10 ± 0.7%	46 ± 1%	74 ± 2%

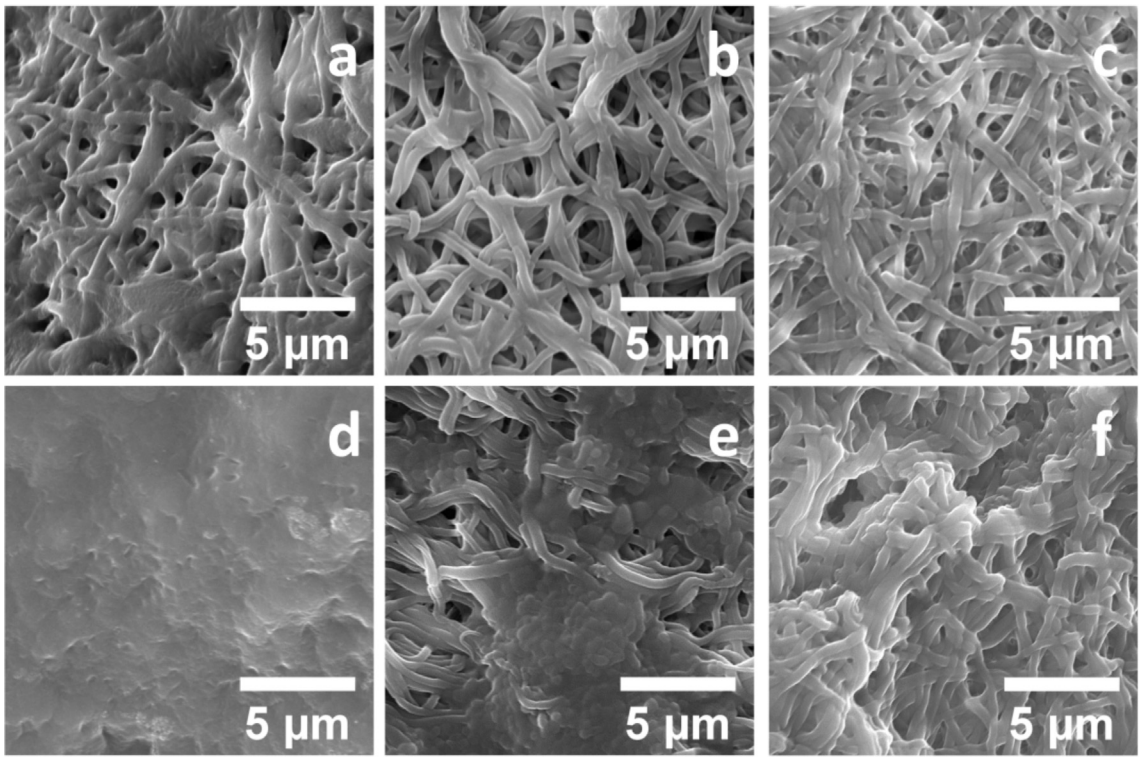

Fig. 5. SEM images of SF-alb-hPL mats with different crystallinity. Micrographs a, b and c depict fiber morphology for the mats with crystallinity of 22%, 35% and 45% respectively, incubated in PBS for 1month. Micrographs d, e and f, show the resulting morphology of mats at equal crystallinity after incubation with Protease XIV (6.25 mU/mg_{fibers}).

4. Discussion

Silk fibroin electrospun fibers, were fabricated from the aqueous solution of fibroin, using PEO to facilitate the process, following a strategy adopted in previous works [54,64–66]. This procedure proved to be effective even for high loading of hPL. To have well-formed submicron fibers, the parameters were adjusted to account for the presence of meta-stable, complex composition of hPL. Since albumin is a component of the hPL (as reported in literature and confirmed in Fig. S3), the fluorescently tagged FITC-albumin was encapsulated in the fibers and used as a tracker because of its easier detection [63]. The homogeneous encapsulation of FITC-albumin in SF-alb and SF-alb-hPL suggested a homogeneous loading of hPL in the electrospun mats as well. In addition, the confirmation of the hPL encapsulation was demonstrated with the ELISA analysis, which detected the PDGF and TGF-β1, and by the *in vitro* experiments in results Section 3.3.

Several studies have shown that the mechanism for degradation of silk fibroin depends on its crystallinity [71]. At low crystallinity (<20%), a fast dissolution is the main pathway for degradation, while, when the crystalline phase is increased (>40%), the main pathway accountable for the degradation is the proteolysis, otherwise the dissolution only accounts for 4% of the mass [29,31–33,71–73,75]. The material's integrity is intertwined with the release of drugs from silk fibroin matrices: for amorphous fibroin, the release was dictated by the dissolution of the material, while for fibroin with high β-sheets content the kinetic depended on the molecular weight of the drug and on the degradation of the silk matrix. A schematic depicting these two mechanisms is reported in Fig. 6. Through the water vapor treatment, a fine control on the fibroin crystallinity was ensured, enabling a tool to tune the release time of FITC-albumin, PDGF and TGF-β1 from the electrospun samples (SF-alb, SF-alb-hPL and SF-hPL) over a large range of time scales. In fact, the results reported in Fig. 4, Fig. 7 and Fig. S7 suggested that, the release kinetics of albumin, PDGF and TGF-β1 were mostly dictated by the fibroin matrix and its crystallinity degree. In previous works by Hines and Kaplan [32,33], the release of small molecules from silk fibroin films was characterized. Two sequential steps were hypothesized: an initial release controlled by the diffusion of the molecules within the fibroin matrix, followed by a second step in which the release from the silk fibroin film was supposed to be controlled by the degradation of the polymeric matrix. In addition, by studying the effect of molecular weight, they showed that the diffusion of small molecules was less affected by the crystallinity than the diffusion of higher molecular weight ones. The results of this study support the proposed

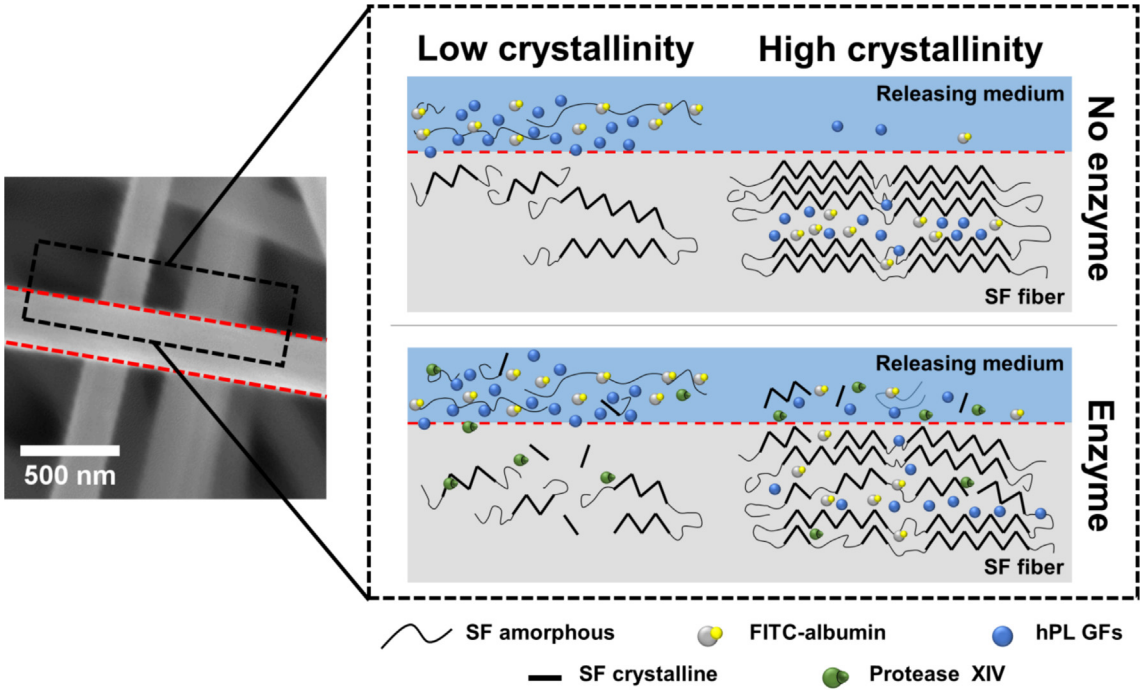

Fig. 6. Proposed mechanism of controlled release from silk fibroin fibrous mats, considering the different silk fibroin crystallinity degree and the presence of the enzymatic activity. Low crystalline samples completely dissolved during the burst release, while the highly crystalline samples featured a reduced release due to the presence of the crystalline domains which impaired the diffusion of the FITC-albumin molecules. After the burst release, for the highly crystalline mats, when the enzyme degradation is not present, the molecules would remain entrapped in the fibroin matrix, whereas, by adding an enzyme, the degradation of the crystalline domain induces the release of the FITCalbumin and the other molecules embedded in it. Therefore, crystallinity also appeared to affect this second release step. In fact, by increasing the crystallinity, the supramolecular interactions in the amorphous silk fibroin increases, such to create a more organized structure, which retards the passage of the enzyme through the crystalline domains. This leads to a slower degradation rate of the fibers during the release process, inducing a crystallinity-dependent release.

Table 2
Summary of the burst release of the PDGF, TGF-β1 and FITC-albumin reported Fig. 7. The data were obtained in the absence of the enzyme.

Crystallinity	PDGF	TGF-β1	FITC-albumin
20%	97 ± 4%	90 ± 0.1%	98 ± 2%
35%	78 ± 9%	40 ± 12%	40 ± 4%
44%	62 ± 3%	12 ± 2%	10 ± 0.1%

model, adding that, after the initial burst, the degradation of the silk fibroin matrix plays an important role in determining the release: as shown in Fig. S7, in the absence of a proteolytic enzyme, the release was inhibited after the first 24 h. The degradation-dependent release, hypothesized by Hines and Kaplan, is shown in this work for the first time to be able to support a sustained release. This degradation-dependent release was more relevant for higher molecular weight molecules like TGF-β1 and albumin but, to a minor degree, it was observed for the smaller PDGF as well. In fact, the mechanism for the release was different for the two growth factors: the burst release was higher for the PDGF, indicating a more diffusion-driven release, while TGF-β1 showed a behavior similar to that was observed for albumin, suggesting a release dominated by the silk fibroin degradation. It is worth noting that for PDGF, even if the diffusion is the main mechanism for release, a significant portion (40%) remains entrapped in the matrix at high silk fibroin crystallinity.

Nultsch *et al.* [56] showed that the release kinetic can be affected by the molecules' charge (or their isoelectric points, IP).

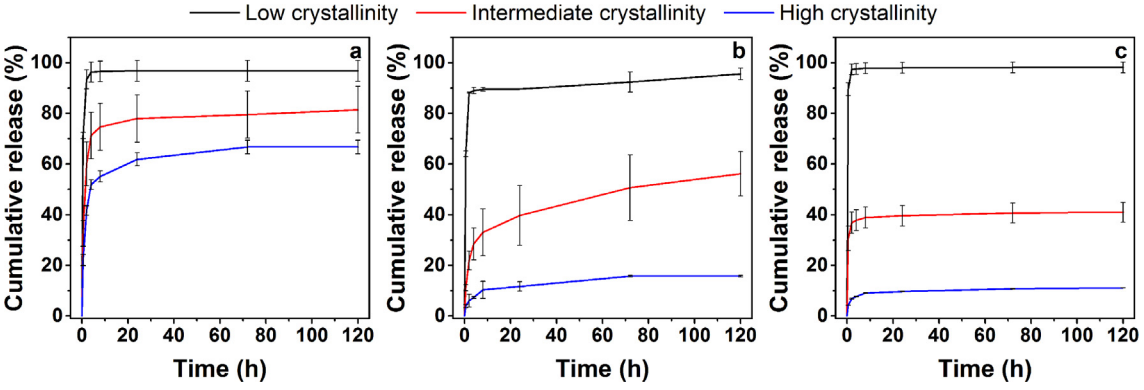

Fig. 7. Release kinetics of the first 120 h of (a) PDGF, (b) TGF-β1 and (c) FITC-albumin from fibrous samples at three different crystallinities. The experiments were performed without the enzyme. Particularly, the data of PDGF and TGF-β1 were obtained by using the ELISA kits, while the ones of the FITC-albumin by using the absorbance for calculating the concentration released.

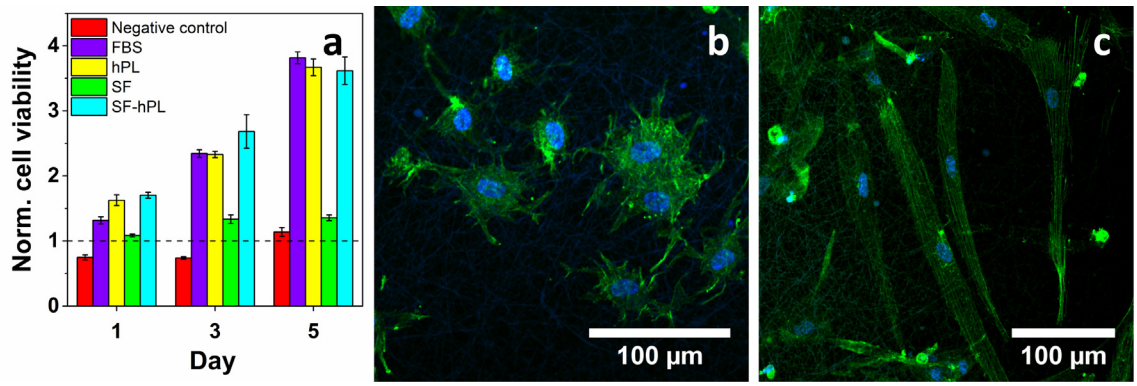

Fig. 8. a) Viability of HDFa cells treated either with 250 µg/mL of hPL or with the extracts of SF and SF-hPL fibers. The values were normalized with respect to the absorbance value of the cells before the treatments, which is showed as a dashed line in the graph; the cells in presence of the hPL from SF-hPL (SF-hPL) showed an increase in viability similar to those grown with hPL dissolved in serum-free medium (hPL) ($p > 0.05$), during all the experiment; SF-hPL cells had a viability statistically higher than those cultivated with SF extracts ($p < 0.0001$) during the five days; b) and c) Confocal images of HDFa cells seeded onto the SF and SF-hPL fibrous mats at 5 days of culture. F-actin is stained with the Alexa-fluor phalloidin (green), while nuclei are stained with DAPI (blue). (For interpretation of the references to colour in this figure legend, the reader is referred to the web version of this article.)

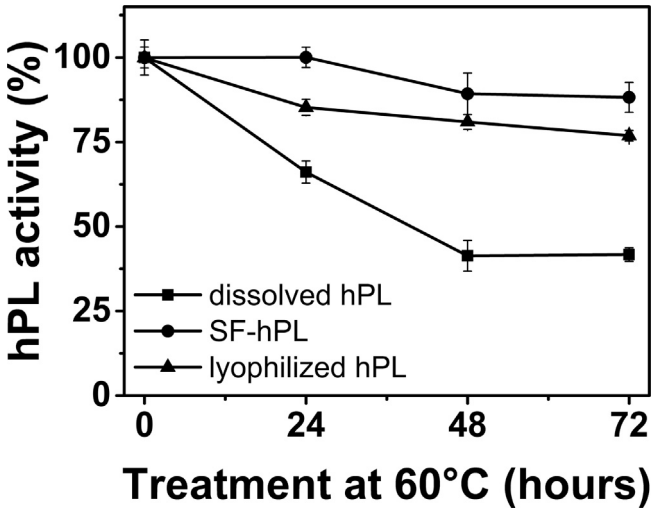

Fig. 9. hPL activity of dissolved hPL, lyophilized hPL and hPL released from SF-hPL matrices after the accelerated stability test. The activity of the hPL released from the fibers after 3 days of thermal treatment had an activity statistically higher activity than the lyophilized hPL ($p < 0.05$) and dissolved hPL ($p < 0.0001$).

Table 3
FITC-albumin releasing rate from silk fibroin fibrous mats at different crystallinity. The rates derive from the graph in Fig. 4.

Releasing rate of FITC-albumin			
	High crystallinity	Intermediate crystallinity	Low crystallinity
Burst 24 h (%/h)	0.4	2	4
1–7 day (%/d)	1	2	–
8–20 days (%/d)	1.5	0.8	–
21 day-exhaustion (%/d)	0.4	0.1	–

Comparing the release kinetics of Albumin (IP = 4.7), PDGF (IP = 9.3) and TGF-β1 (IP = 8.83) [76–79], the effect of charge was not evident.

Thus, for hPL proteins with molecular weight similar to albumin, the release kinetic during the burst phase (0–24 h), the degradation phase (24 h to 7 days) and the sustained degradation (8 days to exhaustion) are reported in Table 3. The rates have been obtained from the graph in Fig. 4. These results showed how the release of drugs can be tuned from few hours for the low crystalline silk fibroin (<24% crystallinity), up to 20 days for the intermediate crystalline samples (between 25% and 35% crystallinity), and a sustained release for up to 100 days for the highly crystalline silk fibroin (>36% crystallinity).

Viability assays performed on the HDFa cells, reported in Fig. 8a, demonstrated that the labile growth factors and cytokines present in hPL are still active after all the fabrication steps. Moreover, HDFa cells seeded onto SF-hPL fibers were able to successfully attach on the matrix, acquiring an elongated morphology which was kept by the cells during all the 5 days of growth (Fig. 8b, c and S10). As shown by Barsotti *et al.* [46] and Anitua *et al.* [74], platelets-derived proteins induced similar changes on dermal fibroblast. This morphology was hypothesized to be associated to cell polarization, a complex process involved in cell migration and wound closure [47].

The preservation of the hPL growth factors activity is of crucial importance not only in the short term of usage, when applied as wound management device, but also in the long term of storage after the fabrication. Nowadays, the general usage of the platelets-derived factors is in a gel form, which needs to be prepared immediately before the treatment [51]. This procedure is time consuming, difficult and only accessible to qualified operators. Thus, the possibility of having a hPL-encapsulated device as a ready-to-use patch should simplify the operations. Given the meta-stability of the growth factors, an improved device should be able to protect and preserve the biological activity of the hPL proteins, in the long term. Fibroin is known to be able to preserve growth factors and enzymes, and to stabilize blood [16–18,21–27]. As highlighted in Fig. 9, hPL released from SF-hPL patches was able to increase cell viability after 3 days of thermal stress, demonstrating the protective role of the fibroin towards the hPL proteins. These results show that the SF-hPL device, in its ready-to-use form, has a stability that is even better than the lyophilized form of hPL. This entails the possibility that SF-hPL devices could be prepared in advance, simplifying their conservation and facilitating their use.

5. Conclusions

The work has demonstrated that electrospun silk fibroin fibers encapsulating the hPL can be fabricated with high loading efficiency: 5% (w/w) of the total mass of the fibers. In addition, the study has shown that silk fibroin can encapsulate hPL and that

the release can be modulated by controlling the silk fibroin's crystallinity using a simple and mild water vapor treatment. The tunability of the release, mediated by the crystallinity, was demonstrated and, for the first time, characterized for such long kinetics. Surprisingly, the crystallinity was able to tune the release of albumin in a range spanning from few hours to almost 3 months. Furthermore, the hPL released from the fibers retained its biological activity, sustaining the HDFa cell growth *in vitro* for up to 5 days. Interestingly, hPL-treated cells appeared to acquire a more polarized morphology, typical of migrating cells that are involved in the wound closure. Finally, the work demonstrated that silk fibroin has a positive protective effect on the hPL, improving their stability at high temperature, suggesting that the electrospun device would have an improved shelf life granted by the silk fibroin matrix.

The proposed engineered fibers could facilitate the use of hPL for wound healing and in medical procedures in which hPL gels are currently used. Electrospun patches are readily applicable to the wound site, similarly to a gauze, could have a predetermined release kinetic and could be prepared and store as ready-to-use devices thanks to the preservation of the hPL activity and the prolonged shelf life granted by the silk matrix.

A more precise knowledge of the growth factors' release and their biological activity *in vitro* and *in vivo*, could lead to the exploit of the facile usage, tunable degradation and sustained release in different applications from wound healing to regenerative medicine.

Acknowledgments

This work was made possible by the Biorigen s.r.l., which granted the hPL. The authors would thank Dr. Giulia Suarato, Dr. Tiziano Catelani and Dr. Fabrizio Schipani for their precious suggestions and technical support.

Appendix A. Supplementary data

Supplementary data associated with this article can be found, in the online version, at https://doi.org/10.1016/j.actbio.2018.04.025.

References

[1] G.H. Altman, F. Diaz, C. Jakuba, T. Calabro, R.L. Horan, J. Chen, H. Lu, J. Richmond, D.L. Kaplan, Silk-based biomaterials, Biomaterials 24 (2003) 401–416, https://doi.org/10.1016/S0142-9612(02)00353-8.

[2] C. Vepari, D.L. Kaplan, Silk as a biomaterial, Prog. Polym. Sci. 32 (2007) 991–1007, https://doi.org/10.1016/j.progpolymsci.2007.05.013.

[3] D.N. Rockwood, R.C. Preda, T. Yücel, X. Wang, M.L. Lovett, D.L. Kaplan, Materials fabrication from Bombyx mori silk fibroin, Nat. Protoc. 6 (2011) 1612–1631, https://doi.org/10.1038/nprot.2011.379.

[4] B. Kundu, R. Rajkhowa, S.C. Kundu, X. Wang, Silk fibroin biomaterials for tissue regenerations, Adv. Drug Deliv. Rev. (2013), https://doi.org/10.1016/j.addr.2012.09.043.

[5] E. Wenk, H.P. Merkle, L. Meinel, Silk fibroin as a vehicle for drug delivery applications, J. Control. Release Off. J. Control. Release Soc. 150 (2011) 128–141, https://doi.org/10.1016/j.jconrel.2010.11.007.

[6] A.N. Mitropoulos, G. Perotto, S. Kim, B. Marelli, D.L. Kaplan, F.G. Omenetto, Synthesis of silk fibroin Micro- and submicron spheres using a Co-flow capillary device, Adv. Mater. 26 (2014) 1105–1110, https://doi.org/10.1002/adma.201304244.

[7] F.P. Seib, G.T. Jones, J. Rnjak-Kovacina, Y. Lin, D.L. Kaplan, pH-Dependent anticancer drug release from silk nanoparticles, Adv. Healthc. Mater. 2 (2013) 1606–1611, https://doi.org/10.1002/adhm.201300034.

[8] V. Catto, S. Farè, I. Cattaneo, M. Figliuzzi, A. Alessandrino, G. Freddi, A. Remuzzi, M.C. Tanzi, Small diameter electrospun silk fibroin vascular grafts: mechanical properties, in vitro biodegradability, and in vivo biocompatibility, Mater. Sci. Eng. C. 54 (2015) 101–111, https://doi.org/10.1016/J.MSEC.2015.05.003.

[9] C.Z. Zhou, F. Confalonieri, N. Medina, Y. Zivanovic, C. Esnault, T. Yang, M. Jacquet, J. Janin, M. Duguet, R. Perasso, Z.G. Li, Fine organization of Bombyx mori fibroin heavy chain gene, Nucleic Acids Res. 28 (2000) 2413–2419.

[10] Q. Lu, X. Hu, X. Wang, J.A. Kluge, S. Lu, P. Cebe, D.L. Kaplan, Water-insoluble silk films with silk I structure, Acta Biomater. 6 (2010) 1380–1387, https://doi.org/10.1016/j.actbio.2009.10.041.

[11] M. Wang, H.J. Jin, D.L. Kaplan, G.C. Rutledge, Mechanical properties of electrospun silk fibers, Macromolecules 37 (2004) 6856–6864, https://doi.org/10.1021/ma048988v.

[12] G. Perotto, Y. Zhang, D. Naskar, N. Patel, D.L. Kaplan, S.C. Kundu, F.G. Omenetto, The optical properties of regenerated silk fibroin films obtained from different sources, Appl. Phys. Lett. 111 (2017) 103702, https://doi.org/10.1063/1.4998950.

[13] X. Hu, K. Shmelev, L. Sun, E.-S. Gil, S.-H. Park, P. Cebe, D.L. Kaplan, Regulation of silk material structure by Temperature-controlled water vapor annealing, Biomacromolecules 12 (2011) 1686–1696, https://doi.org/10.1021/bm200062a.

[14] A. Motta, D. Maniglio, C. Migliaresi, H.-J. Kim, X. Wan, X. Hu, D.L. Kaplan, Silk fibroin processing and thrombogenic responses, J. Biomater. Sci. Polym. Ed. 20 (2009) 1875–1897, https://doi.org/10.1163/156856208X399936.

[15] M. Floren, W. Bonani, A. Dharmarajan, A. Motta, C. Migliaresi, W. Tan, Human mesenchymal stem cells cultured on silk hydrogels with variable stiffness and growth factor differentiate into mature smooth muscle cell phenotype, Acta Biomater. 31 (2016) 156–166, https://doi.org/10.1016/j.actbio.2015.11.051.

[16] A.N. Mitropoulos, B. Marelli, G. Perotto, J. Amsden, D.L. Kaplan, F.G. Omenetto, H. Lu, J. Richmond, D.L. Kaplan, J.A. Rogers, D.L. Kaplan, F.G. Omenetto, Towards the fabrication of biohybrid silk fibroin materials: entrapment and preservation of chloroplast organelles in silk fibroin films, RSC Adv. 6 (2016) 72366–72370, https://doi.org/10.1039/C6RA13228F.

[17] E.M. Pritchard, P.B. Dennis, F. Omenetto, R.R. Naik, D.L. Kaplan, Physical and chemical aspects of stabilization of compounds in silk, Biopolymers 97 (2012) 479–498, https://doi.org/10.1002/bip.22026.

[18] J.A. Kluge, A.B. Li, B.T. Kahn, D.S. Michaud, F.G. Omenetto, D.L. Kaplan, Silk-based blood stabilization for diagnostics, Proc. Natl. Acad. Sci. 113 (2016) 5892–5897, https://doi.org/10.1073/pnas.1602493113.

[19] F.P. Seib, D.L. Kaplan, Doxorubicin-loaded silk films: Drug-silk interactions and in vivo performance in human orthotopic breast cancer, Biomaterials 33 (2012) 8442–8450, https://doi.org/10.1016/j.biomaterials.2012.08.004.

[20] S. Hofmann, C.T. Wong Po Foo, F. Rossetti, M. Textor, G. Vunjak-Novakovic, D.L. Kaplan, H.P. Merkle, L. Meinel, Silk fibroin as an organic polymer for controlled drug delivery, J. Control. Release 111 (2006) 219–227, https://doi.org/10.1016/j.jconrel.2005.12.009.

[21] S. Putthanarat, R.K. Eby, R.R. Naik, S.B. Juhl, M.A. Walker, E. Peterman, S. Ristich, J. Magoshi, T. Tanaka, M.O. Stone, B.L. Farmer, C. Brewer, D. Ott, Nonlinear optical transmission of silk/green fluorescent protein (GFP) films, Polymer (Guildf) 45 (2004) 8451–8457, https://doi.org/10.1016/j.polymer.2004.10.014.

[22] J. Kikuchi, Y. Mitsui, T. Asakura, K. Hasuda, H. Araki, K. Owaku, Spectroscopic investigation of tertiary fold of staphylococcal protein A to explore its engineering application, Biomaterials 20 (1999) 647–654, https://doi.org/10.1016/S0142-9612(98)00220-8.

[23] Q. Lu, X. Wang, X. Hu, P. Cebe, F. Omenetto, D.L. Kaplan, Stabilization and release of enzymes from silk films, Macromol. Biosci. 10 (2010) 359–368, https://doi.org/10.1002/mabi.200900388.

[24] Y. Wu, Q. Shen, S. Hu, Direct electrochemistry and electrocatalysis of Hemeproteins in regenerated silk fibroin film, Anal. Chim. Acta. 558 (2006) 179–186, https://doi.org/10.1016/j.aca.2005.11.031.

[25] J. Zhang, E. Pritchard, X. Hu, T. Valentin, B. Panilaitis, F.G. Omenetto, D.L. Kaplan, Stabilization of vaccines and antibiotics in silk and eliminating the cold chain, Proc. Natl. Acad. Sci. U.S.A. 109 (2012) 11981–11986, https://doi.org/10.1073/pnas.1206210109.

[26] A.B. Li, J.A. Kluge, N.A. Guziewicz, F.G. Omenetto, D.L. Kaplan, Silk-based stabilization of biomacromolecules, J. Control. Release 219 (2015) 416–430, https://doi.org/10.1016/j.jconrel.2015.09.037.

[27] S. Lu, X. Wang, Q. Lv, X. Hu, N. Uppal, D.L. Kaplan, Stabilization of Enzymes in Silk Films, Biomacromolecules 10 (2009) 1032–1042, https://doi.org/10.1021/bm800956n.Stabilization.

[28] P. Tseng, G. Perotto, B. Napier, P. Riahi, W. Li, E. Shirman, D.L. Kaplan, I.V. Zenyuk, F.G. Omenetto, Silk Fibroin-carbon nanotube composite electrodes for flexible biocatalytic fuel cells, Adv. Electron. Mater. 2 (2016) 1600190, https://doi.org/10.1002/aelm.201600190.

[29] J.H. Kim, C.H. Park, O.-J. Lee, J.-M. Lee, J.W. Kim, Y.H. Park, C.S. Ki, Preparation and in vivo degradation of controlled biodegradability of electrospun silk fibroin nanofiber mats, J. Biomed. Mater. Res. A 100 (2012) 3287–3295, https://doi.org/10.1002/jbm.a.34274.

[30] U.-J. Kim, J. Park, H. Joo Kim, M. Wada, D.L. Kaplan, Three-dimensional Aqueous-derived biomaterial scaffolds from silk fibroin, Biomaterials 26 (2005) 2775–2785, https://doi.org/10.1016/j.biomaterials.2004.07.044.

[31] Y. Wang, D.D. Rudym, A. Walsh, L. Abrahamsen, H.-J. Kim, H.S. Kim, C. Kirker-Head, D.L. Kaplan, In vivo degradation of Three-dimensional silk fibroin scaffolds, Biomaterials 29 (2008) 3415–3428, https://doi.org/10.1016/j.biomaterials.2008.05.002.

[32] D.J. Hines, D.L. Kaplan, Mechanisms of controlled release from silk fibroin films, Biomacromolecules. 12 (2011) 804–812, https://doi.org/10.1021/bm101421r.

[33] D.J. Hines, D.L. Kaplan, Characterization of small molecule controlled release from silk films, Macromol. Chem. Phys. 214 (2013) 280–294, https://doi.org/10.1002/macp.201200407.

[34] J.M. Coburn, E. Na, D.L. Kaplan, Modulation of vincristine and doxorubicin binding and release from silk films, J. Control. Release 220 (2015) 229–238, https://doi.org/10.1016/j.jconrel.2015.10.035.

[35] X. Wang, E. Wenk, A. Matsumoto, L. Meinel, C. Li, D.L. Kaplan, Silk microspheres for encapsulation and controlled release, J. Control. Release 117 (2007) 360–370, https://doi.org/10.1016/j.jconrel.2006.11.021.
[36] B. Chiu, J. Coburn, M. Pilichowska, C. Holcroft, F.P. Seib, A. Charest, D.L. Kaplan, Surgery combined with controlled-release doxorubicin silk films as a treatment strategy in an orthotopic neuroblastoma mouse model, Br. J. Cancer 111 (2014) 708–715, https://doi.org/10.1038/bjc.2014.324.
[37] J.S. Boateng, K.H. Matthews, H.N.E. Stevens, G.M. Eccleston, Wound healing dressings and drug delivery systems: a review, J. Pharm. Sci. 97 (2008) 2892–2923, https://doi.org/10.1002/jps.21210.
[38] A. Buckley, J.M. Davidson, C.D. Kamerath, T.B. Wolt, S.C. Woodward, Sustained release of epidermal growth factor accelerates wound repair, Proc. Natl. Acad. Sci. U.S.A. 82 (1985) 7340–7344.
[39] M.H. Sheridan, L.D. Shea, M.C. Peters, D.J. Mooney, Bioabsorbable polymer scaffolds for tissue engineering capable of sustained growth factor delivery, J. Control. Release 64 (2000) 91–102.
[40] S.D. Putney, P.A. Burke, Improving protein therapeutics with sustained-release formulations, Nat. Biotechnol. 16 (1998) 153–157, https://doi.org/10.1038/nbt0298-153.
[41] N.T. Bennett, G.S. Schultz, Growth factors and wound healing: Part II. Role in normal and chronic wound healing, Am. J. Surg. 166 (1993) 74–81.
[42] N. Morimoto, K. Yoshimura, M. Niimi, T. Ito, R. Aya, J. Fujitaka, H. Tada, S. Teramukai, T. Murayama, C. Toyooka, K. Miura, S. Takemoto, N. Kanda, K. Kawai, M. Yokode, A. Shimizu, S. Suzuki, Novel collagen/gelatin scaffold with sustained release of basic fibroblast growth factor: clinical trial for chronic skin ulcers, Tissue Eng. Part A 19 (2013) 1931–1940, https://doi.org/10.1089/ten.tea.2012.0634.
[43] S.H. Zaky, A. Ottonello, P. Strada, R. Cancedda, M. Mastrogiacomo, Platelet lysate favours in vitro expansion of human bone marrow stromal cells for bone and cartilage engineering, J. Tissue Eng. Regen. Med. 2 (2008) 472–481, https://doi.org/10.1002/term.119.
[44] A. Muraglia, M.R. Todeschi, A. Papait, A. Poggi, R. Spanò, P. Strada, R. Cancedda, M. Mastrogiacomo, Combined platelet and plasma derivatives enhance proliferation of stem/progenitor cells maintaining their differentiation potential, Cytotherapy. 17 (2015) 1793–1806, https://doi.org/10.1016/j.jcyt.2015.09.004.
[45] A. Muraglia, C. Ottonello, R. Spanò, B. Dozin, P. Strada, M. Grandizio, R. Cancedda, M. Mastrogiacomo, Biological activity of a standardized Freeze-dried platelet derivative to be used as cell culture medium supplement, Platelets 25 (2014) 211–220, https://doi.org/10.3109/09537104.2013.803529.
[46] M. Chiara Barsotti, P. Losi, E. Briganti, E. Sanguinetti, A. Magera, T. Al Kayal, R. Feriani, R. Di Stefano, G. Soldani, Effect of platelet lysate on human cells involved in different phases of wound healing, PLoS One 8 (2013), https://doi.org/10.1371/journal.pone.0084753.
[47] R. El Backly, V. Ulivi, L. Tonachini, R. Cancedda, F. Descalzi, M. Mastrogiacomo, Platelet lysate induces in vitro wound healing of human keratinocytes associated with a strong proinflammatory response, Tissue Eng. Part A 17 (2011) 1787–1800, https://doi.org/10.1089/ten.tea.2010.0729.
[48] H.S. Yang, J. Shin, S.H. Bhang, J.Y. Shin, J. Park, G. Il Im, C.S. Kim, B.S. Kim, Enhanced skin wound healing by a sustained release of growth factors contained in Platelet-rich plasma, Exp. Mol. Med. 43 (2011) 622–629, https://doi.org/10.3858/emm.2011.43.11.070.
[49] R.M. El Backly, S.H. Zaky, A. Muraglia, L. Tonachini, F. Brun, B. Canciani, D. Chiapale, F. Santolini, R. Cancedda, M. Mastrogiacomo, A Platelet-rich Plasma-based membrane as a periosteal substitute with enhanced osteogenic and angiogenic properties: a new concept for bone repair, Tissue Eng. Part A 19 (2013) 152–165, https://doi.org/10.1089/ten.TEA.2012.0357.
[50] D.R. Knighton, K.F. Ciresi, V.D. Fiegel, L.L. Austin, E.L. Butler, Classification and treatment of chronic nonhealing wounds. Successful treatment with autologous Platelet-derived wound healing factors (PDWHF), Ann. Surg. 204 (1986) 322–330.
[51] R. Spanò, A. Muraglia, M.R. Todeschi, M. Nardini, P. Strada, R. Cancedda, M. Mastrogiacomo, Platelet-rich plasma-based bioactive membrane as a new advanced wound care tool, J. Tissue Eng. Regen. Med. (2017), https://doi.org/10.1002/term.2357. n/a-n/a.
[52] E. Anitua, J.J. Aguirre, J. Algorta, E. Ayerdi, A.I. Cabezas, G. Orive, I. Andia, Effectiveness of autologous preparation rich in growth factors for the treatment of chronic cutaneous ulcers, J. Biomed. Mater. Res. Part B Appl. Biomater. 84B (2008) 415–421, https://doi.org/10.1002/jbm.b.30886.
[53] N. Fekete, M. Gadelorge, D. Fürst, C. Maurer, J. Dausend, S. Fleury-Cappellesso, V. Mailänder, R. Lotfi, A. Ignatius, L. Sensebé, P. Bourin, H. Schrezenmeier, M.T. Rojewski, Platelet lysate from whole Blood-derived pooled platelet concentrates and apheresis-derived platelet concentrates for the isolation and expansion of human bone marrow mesenchymal stromal cells: production process, content and identification of active comp, Cytotherapy. 14 (2012) 540–554, https://doi.org/10.3109/14653249.2012.655420.
[54] H.-J. Jin, S.V. Fridrikh, G.C. Rutledge, D.L. Kaplan, Electrospinning Bombyx mori silk with Poly(ethylene oxide), Biomacromolecules 3 (2002) 1233–1239, https://doi.org/10.1021/bm025581u.
[55] Y. Kishimoto, H. Morikawa, S. Yamanaka, Y. Tamada, Electrospinning of silk fibroin from all aqueous solution at low concentration, Mater. Sci. Eng. C 73 (2017) 498–506, https://doi.org/10.1016/j.msec.2016.12.113.
[56] K. Nultsch, O. Germershaus, Silk fibroin degumming affects scaffold structure and release of macromolecular drugs, Eur. J. Pharm. Sci. 106 (2017) 254–261, https://doi.org/10.1016/j.ejps.2017.06.012.
[57] I. Pallotta, J.A. Kluge, J. Moreau, R. Calabrese, D.L. Kaplan, A. Balduini, Characteristics of platelet gels combined with silk, Biomaterials 35 (2014) 3678–3687, https://doi.org/10.1016/J.biomaterials.2013.12.065.
[58] P. Zahedi, I. Rezaeian, S.-O. Ranaei-Siadat, S.-H. Jafari, P. Supaphol, A review on wound dressings with an emphasis on electrospun nanofibrous polymeric bandages, Polym. Adv. Technol. 21 (2010) 77–95, https://doi.org/10.1002/pat.1625.
[59] M. Abrigo, S.L. McArthur, P. Kingshott, Electrospun nanofibers as dressings for chronic wound care: advances, challenges, and future prospects, Macromol. Biosci. 14 (2014) 772–792, https://doi.org/10.1002/mabi.201300561.
[60] H. Hajiali, M. Summa, D. Russo, A. Armirotti, V. Brunetti, R. Bertorelli, A. Athanassiou, E. Mele, Alginate–lavender nanofibers with antibacterial and anti-inflammatory activity to effectively promote burn healing, J. Mater. Chem. B 4 (2016) 1686–1695, https://doi.org/10.1039/C5TB02174J.
[61] I. Romano, M. Summa, J.A. Heredia-Guerrero, R. Spanò, L. Ceseracciu, C. Pignatelli, R. Bertorelli, E. Mele, A. Athanassiou, Fumarate-loaded electrospun nanofibers with Anti-inflammatory activity for fast recovery of mild skin burns, Biomed. Mater. 11 (2016) 41001, https://doi.org/10.1088/1748-6041/11/4/041001.
[62] P. Wolfe, S.A. Sell, J. Ericksen, D. Simpson, Bowlin, The creation of electrospun nanofibers from platelet rich plasma, J. Tissue Sci. Eng. 24172 (2011) 1072157–1077552, https://doi.org/10.4172/2157-7552.1000107.
[63] Y.D. Shanskii, N.S. Sergeeva, I.K. Sviridova, M.S. Kirakozov, V.A. Kirsanova, S.A. Akhmedova, A.I. Antokhin, V.I. Chissov, Human platelet lysate as a promising Growth-stimulating additive for culturing of stem cells and other cell types, Bull. Exp. Biol. Med. 156 (2013) 146–151, https://doi.org/10.1007/s10517-013-2298-7.
[64] J. Chutipakdeevong, U.R. Ruktanonchai, P. Supaphol, Process optimization of electrospun silk fibroin fiber mat for accelerated wound healing, J. Appl. Polym. Sci. 130 (2013) 3634–3644, https://doi.org/10.1002/app.39611.
[65] E.S. Gil, B. Panilaitis, E. Bellas, D.L. Kaplan, Functionalized silk biomaterials for wound healing, Adv. Healthc. Mater. 2 (2013) 206–217, https://doi.org/10.1002/adhm.201200192.
[66] A. Schneider, X.Y. Wang, D.L. Kaplan, J.A. Garlick, C. Egles, Biofunctionalized electrospun silk mats as a topical bioactive dressing for accelerated wound healing, Acta Biomater. 5 (2009) 2570–2578, https://doi.org/10.1016/j.actbio.2008.12.013.
[67] S. Guzman-Puyol, J.A. Heredia-Guerrero, L. Ceseracciu, H. Hajiali, C. Canale, A. Scarpellini, R. Cingolani, I.S. Bayer, A. Athanassiou, E. Mele, Low-cost and effective fabrication of biocompatible nanofibers from silk and Cellulose-rich materials, ACS Biomater. Sci. Eng. 2 (2016) 526–534, https://doi.org/10.1021/acsbiomaterials.5b00500.
[68] X. Hu, D. Kaplan, P. Cebe, Determining Beta-sheet crystallinity in fibrous proteins by thermal analysis and infrared spectroscopy, Macromolecules 39 (2006) 6161–6170, https://doi.org/10.1021/ma0610109.
[69] A.J. Meinel, K.E. Kubow, E. Klotzsch, M. Garcia-Fuentes, M.L. Smith, V. Vogel, H. P. Merkle, L. Meinel, Optimization strategies for electrospun silk fibroin tissue engineering scaffolds, Biomaterials 30 (2009) 3058–3067, https://doi.org/10.1016/j.biomaterials.2009.01.054.
[70] B.M. Min, L. Jeong, K.Y. Lee, W.H. Park, Regenerated silk fibroin nanofibers: water Vapor-induced structural changes and their effects on the behavior of normal human cells, Macromol. Biosci. 6 (2006) 285–292, https://doi.org/10.1002/mabi.200500246.
[71] F.P. Seib, D.L. Kaplan, Silk for drug delivery applications: Opportunities and challenges, Isr. J. Chem. 53 (2013) 756–766, https://doi.org/10.1002/ijch.201300083.
[72] E.S. Gil, S.H. Park, X. Hu, P. Cebe, D.L. Kaplan, Impact of sterilization on the enzymatic degradation and mechanical properties of silk biomaterials, Macromol. Biosci. 14 (2014) 257–269, https://doi.org/10.1002/mabi.201300321.
[73] J. Zhou, C. Cao, X. Ma, L. Hu, L. Chen, C. Wang, In vitro and in vivo degradation behavior of Aqueous-derived electrospun silk fibroin scaffolds, Polym. Degrad. Stab. 95 (2010) 1679–1685, https://doi.org/10.1016/j.polymdegradstab.2010.05.025.
[74] E. Anitua, A. Pino, G. Orive, Plasma rich in growth factors promotes dermal fibroblast proliferation, migration and biosynthetic activity, J. Wound Care 25 (2016) 680–687, https://doi.org/10.12968/jowc.2016.25.11.680.
[75] M. Li, M. Ogiso, N. Minoura, Enzymatic degradation behavior of porous silk fibroin sheets, Biomaterials 24 (2003) 357–365, https://doi.org/10.1016/S0142-9612(02)00326-5.
[76] C.R. Carlin, B.B. Knowles, Identity of human epidermal growth factor (EGF) receptor with glycoprotein SA-7: evidence for differential phosphorylation of the two components of the EGF receptor from A431 cells, Proc. Natl. Acad. Sci. U.S.A. 79 (1982) 5026–5030, https://doi.org/10.1074/jbc.M403114200. Epidermal.
[77] L.M. Mullen, S.M. Best, R.A. Brooks, S. Ghose, J.H. Gwynne, J. Wardale, N. Rushton, R.E. Cameron, Binding and release characteristics of Insulin-like growth Factor-1 from a Collagen-glycosaminoglycan scaffold, Tissue Eng. Part C Methods 16 (2010) 1439–1448, https://doi.org/10.1089/ten.tec.2009.0806.
[78] C.H. Heldin, A. Johnsson, B. Ek, S. Wennergren, L. Rönnstrand, A. Hammacher, B. Faulders, A. Wasteson, B. Westermark, Purification of human platelet-derived growth factor, Methods Enzymol. 147 (1987) 3–13.
[79] P. Vuorela-Vepsalainen, H. Alfthan, A. Orpana, K. Alitalo, U.H. Stenman, E. Halmesmaki, Vascular endothelial growth factor is bound in amniotic fluid and maternal serum, Hum Reprod. 14 (1999) 1346–1351.